



Synthesis, characterization, and swelling kinetic study of porous superabsorbent hydrogel nanocomposite based on sulfonated carboxymethylcellulose and silica nanoparticles

Ali Olad¹ · Hamid Zebhi¹ · Dariush Salari¹ · Abdolreza Mirmohseni¹ · Adel Reyhanitabar²

Published online: 4 December 2017

© Springer Science+Business Media, LLC, part of Springer Nature 2017

Abstract

New superabsorbent nanocomposite was synthesized by free-radical graft polymerization of sulfonated-carboxymethyl cellulose (SCMC) with acrylic acid (AA) in the presence of polyvinylpyrrolidone (PVP) and silica nanoparticles. Carboxymethyl cellulose (CMC) was first sulfonated using chlorosulfonic acid, and then AA monomers were grafted onto SCMC. FTIR results confirmed that sulfonation of CMC as well as grafting of AA monomers onto SCMC has been performed successfully. Moreover, the presence of silica nanoparticles into superabsorbent nanocomposite was evaluated with EDX analysis. The element mappings show a homogenous distribution of silica nanoparticles throughout the hydrogel nanocomposite. SEM images exhibited porous morphology for hydrogel nanocomposite, which was due to the incorporation of PVP in its network. The experimental findings from TGA analysis indicated that incorporation of PVP and silica nanoparticles into the hydrogel network improved thermal stability of superabsorbent nanocomposite. Swelling kinetic studies revealed that superabsorbent nanocomposite hydrogel had higher equilibrium swelling capacity and swelling rate compared with the neat hydrogel sample. Besides that, superabsorbent nanocomposite depicted excellent salt and pH-sensitive behavior in different saline and pH solutions. As a consequence, this hydrogel nanocomposite acts as useful water reservoir, which might be most profitable in agricultural applications.

Keywords Superabsorbent nanocomposite · Sulfonated CMC · Swelling kinetic · Silica nanoparticles

1 Introduction

Superabsorbent hydrogels (SHs) are cross-linked polymeric networks that can absorb large amounts of aqueous solutions due to the presence of hydrophilic functional groups in their backbone [1]. These materials possess variable industrial applications because of their sensitivity to some environmental parameters such as pH, temperature, and solvent composition. For example, water retention property and thereafter slow release of water from swollen SHs make them as good water retention systems for agricultural

applications [2–5]. SHs are divided into two categories including, natural and synthetic based polymers. Some properties of natural-based SHs (based on the natural polymers like, proteins, starch, chitosan, cellulose, carrageenan, and sodium alginate) such as biocompatibility, non-toxicity, and biodegradability make them more useable [6, 7]. Cellulose is one of the cheapest natural polymers that is used extensively in various applications of hydrogels [8–10]. Inter-molecular and intra-molecular hydrogen bonds in cellulose backbone created by own hydroxyl groups considerably reduce its solubility and reactivity. Carboxymethyl cellulose (CMC) is a derivative of cellulose in which hydroxyl group is replaced by carboxyl group. The hydrophilicity of carboxyl groups is higher than that of hydroxyl groups. Thus, water uptake capacity of CMC-based hydrogels will be greater than that of cellulose-based ones [11]. Despite these advantages, CMC-based hydrogels suffer from poor mechanical strength. One of the most promising ways to improve the mechanical properties of CMC-based hydrogels is graft polymerization of acrylic acid, acrylamide and their copolymers onto CMC

✉ Ali Olad
a.olad@yahoo.com

¹ Polymer Composite Research Laboratory, Department of Applied Chemistry, Faculty of Chemistry, University of Tabriz, Tabriz, Iran

² Department of Soil Science, Faculty of Agriculture, University of Tabriz, Tabriz, Iran

chains [12–14]. Moreover, introducing of low cost inorganic nanofillers into hydrogels (especially in natural-based hydrogels) is another method, can improve mechanical and thermal properties as well as reduce final production cost of the neat hydrogels [15–18]. Silica is a basic raw material which can be obtained from incineration of rice husk (RH) [19, 20]. Introducing of silica nanoparticles into neat hydrogel, due to hydrogen bonding interactions among functional groups of the hydrogel and hydroxyl groups of silica nanoparticles, can enhance mechanical strength and thermal stability of pure hydrogel. Pourjavadi et al., synthesized hydrogel composite based on the CMC-g-poly(acrylic acid-co-2-acrylamido-2-methylpropanesulfonic acid)/silica. They showed that the prepared hydrogel composite has higher swelling capacity as well as improved thermal stability compared with pure hydrogel [21]. At the same time, using water soluble linear nonionic polymers such as polyvinylpyrrolidone (PVP) being compatible with CMC, creates porous hydrogels and increases their water absorption capacity [22]. Roy et al., synthesized CMC and PVP mixed hydrogels [23]. They showed that hydrogel containing PVP/CMC ratio of 20:80 is the best one from water absorbent point of view.

To the best of our knowledge, superabsorbent nanocomposite based on sulfonated CMC and silica nanoparticles has not been investigated so far. Therefore, in this study we encouraged to synthesize a novel SCMC-g-poly(acrylic acid)/PVP/silica (Hyd/PVP/silica) superabsorbent nanocomposite. For this purpose, CMC was first sulfonated by chlorosulfonic acid in dimethyl formamide (DMF) solvent, and then SCMC was used for synthesis of superabsorbent hydrogels. The effect of PVP and silica nanoparticle on the thermal stability, water absorption capacity, and swelling kinetics of the hydrogels was investigated. Moreover, the swelling behavior of the synthesized hydrogels was evaluated in different saline and pH solutions.

2 Experimental

2.1 Materials

Acrylic acid (AA), *N,N'*-methylene bisacrylamide (MBA), ammonium persulfate (APS), sodium hydroxide, chlorosulfonic acid, Polyvinylpyrrolidone (PVP, M_w 25000–30000), and dimethylformamide (DMF) were purchased from Merck company. Carboxymethyl cellulose sodium salt (NaCMC) (> 99.5%) (Viscosity of 1000–1500 mPas for a 4% aqueous solution at 25 °C) was purchased from Fluka BioChemika. Ethanol (96%) was purchased from Mojallali reagent chemicals Co. (Iran, Tabriz). RH was provided from a supplier in Rasht, Iran. All other reactants were of analytical grade and all solutions were prepared with distilled water.

2.2 Sulfonation of CMC

First, 8 ml chlorosulfonic acid (ClSO_3H) was added dropwise into a beaker containing 40 ml dimethylformamide, surrounded by water/ice bath. The prepared solution was charged into round-bottomed flask equipped with magnetic stirrer and reflux condenser. Then, 5 g CMC was added into the prepared mixture and allowed to be stirred at 60 °C for 4 h. The brown-colored solution was cooled down to room temperature and then the solution pH was adjusted in the range of 10–11 by NaOH (1 M). Finally, 50 ml ethanol was added to the mixture as an anti-solvent agent and light brown-colored sediment deposited in the bottom of the flask. In continue, the obtained precipitate was filtered, washed thoroughly with distilled water, and then dried in an oven at 60 °C for 24 h.

2.3 Preparation of silica nanoparticles

Silica nanoparticles were prepared according to our reported procedure [24]. Briefly, RH was washed with distilled water to remove its soil and dust. Then, it was acid-washed in two steps. In the first step, RH was stirred in boiling HCl solution (3% V/V) with the ratio of 50 g L^{-1} for 2 h. The obtained mixture was filtered and then the precipitate was washed with distilled water for several times. Thereafter, the filtered RH was dried in an oven at 100 °C for 24 h. In the second step, the RH was acid-leached by reflux boiling in H_2SO_4 aqueous solution (10% V/V) for 2 h. In continue filtration and drying processes were performed similar to the previous step. Finally, the dried RH sample was calcined in a furnace at 900 °C for 5 h, yielding white-colored ash which contained 90–97% silica.

2.4 Synthesis of Hyd/PVP/silica hydrogels

First, 1 g SCMC was mixed adequately with 30 ml distilled water in a three necked glass round-bottomed flask equipped with a mechanical stirrer, a reflux condenser, and a nitrogen purge line. The prepared mixture was stirred continuously at 40 °C for 10 min to obtain a homogeneous solution. Then, certain amount of PVP (PVP/SCMC weight ratio: 0.5–1.5) and silica nanoparticles (2.5–10 wt%, with respect to SCMC) were added to the prepared solution while stirring. A few minutes later, 7.2 ml of 65% neutralized AA and 0.018 g of cross-linker agent MBA were added to the mixture. After purging with nitrogen to remove the dissolved oxygen, 0.05 g of APS was added to the mixture as initiator agent. Thereafter, temperature of the reaction mixture was raised up to 60 °C and kept at this condition for 4 h to complete the polymerization process. The gel like product was

cut into small pieces, and then it was immersed in ethanol for 24 h to remove unreacted species. Afterwards, the dehydrated hydrogel sample was dried in an oven at 70 °C for 24 h. For comparison, a neat hydrogel sample without addition of PVP and silica nanoparticles was also synthesized similar to the above described method. Table 1 shows the concentration of the components for each hydrogel sample.

2.5 Characterization

The FTIR spectra of CMC, SCMC, silica, Hyd, Hyd/PVP, and Hyd/PVP/silica were recorded by a Bruker Tensor 27 FTIR instrument at the wavenumber range of 400–4000 cm^{-1} using samples which were prepared as KBr pellets. Wide angle X-ray diffraction patterns of silica, Hyd, Hyd/PVP and Hyd/PVP/silica were also recorded using a Siemens D500 X-ray diffractometer (Siemens AG, Karlsruhe, Germany) with Cu $K\alpha$ radiation in 2θ range of 2° – 70° . The surface morphology of SCMC, Hyd, Hyd/PVP and Hyd/PVP/silica was studied using MIRA3 FEG-SEM (Tescan, Czech) scanning electron microscope coupled with an energy dispersive X-ray analyzer (EDX) (Tescan, Czech, model SAMX). Thermal properties of the hydrogels and their water holding capability were estimated by recording thermal gravimetric runs on a Perkin-Elmer TGA-7 thermogravimetric analyzer (PerkinElmer Cetus Instruments, Norwalk, CT) under dry nitrogen flow rate of 50 mL/min, temperature range of 40–620 °C, and at a heating rate of 10 °C min^{-1} .

2.6 Evaluation of swelling kinetic

To investigate the swelling kinetic of the prepared hydrogels, 0.05 g of dried hydrogel sample was transferred into a tea bag and then it was immersed in 400 ml distilled

water for 24 h at room temperature. Then, the swollen hydrogel sample was taken out of the distilled water in certain time intervals and was weighted after removing the surface water by a filter paper. The equilibrium swelling ratio (S_{eq} (g/g)) was calculated using the following equation:

$$S_{\text{eq}}(\text{g/g}) = \frac{W_s - W_d}{W_d} \quad (1)$$

where S_{eq} (g/g) is equilibrium swelling ratio, W_s (g) is the weight of the swollen hydrogel sample, and W_d (g) is the weight of the dry hydrogel sample.

2.7 pH-sensitivity behavior

To investigate the pH sensitivity of hydrogels, various acidic and basic solutions with different pH values ranging from 2 to 12 were prepared by diluting 0.1 M aqueous solutions of NaOH and HCl. Then, 0.05 g of dried hydrogel sample was immersed in solutions with different pH values. Thereafter, the equilibrium swelling ratio was determined similar to the method described in Sect. 2.5.

2.8 Swelling behavior in different saline solutions

To investigate the effect of different saline solutions on the swelling behavior of hydrogels, 0.05 g of dried hydrogel sample was immersed in 1 M aqueous solutions of NaCl, CaCl_2 , and FeCl_3 . The equilibrium swelling capacity was calculated similar to the previously mentioned method.

Table 1 Amount of CMC, AA, MBA, APS, silica nanoparticles and PVP in different formulations

| Sample | CMC (g) | SCMC (g) | MBA (g) | APS (g) | AA (ml) | PVP/SCMC | Nano silica/SCMC (wt%) | Swelling capacity (g/g) |
|--------|---------|----------|---------|---------|---------|----------|------------------------|-------------------------|
| C1 | 1 | – | 0.018 | 0.05 | 7.2 | – | – | 566 |
| C2 | – | 1 | 0.018 | 0.05 | 7.2 | – | – | 650.2 |
| C3 | – | 1 | 0.018 | 0.05 | 7.2 | 0.5 | – | 687 |
| C4 | – | 1 | 0.018 | 0.05 | 7.2 | 0.75 | – | 765 |
| C5 | – | 1 | 0.018 | 0.05 | 7.2 | 1 | – | 887 |
| C6 | – | 1 | 0.018 | 0.05 | 7.2 | 1.25 | – | 723 |
| C7 | – | 1 | 0.018 | 0.05 | 7.2 | 1.5 | – | 587 |
| C8 | – | 1 | 0.018 | 0.05 | 7.2 | 1 | 2.5 | 613 |
| C9 | – | 1 | 0.018 | 0.05 | 7.2 | 1 | 5 | 807 |
| C10 | – | 1 | 0.018 | 0.05 | 7.2 | 1 | 7.5 | 590 |
| C11 | – | 1 | 0.018 | 0.05 | 7.2 | 1 | 10 | 452 |

3 Results and discussion

3.1 Synthesis of Hyd/PVP/silica superabsorbent nanocomposite

The superabsorbent nanocomposite was prepared by free-radical graft polymerization of acrylic acid monomers onto SCMC chains. Polymerization reaction was performed in the presence of APS as an initiator agent, MBA as a cross-linking agent, PVP as interpenetrating polymer, and silica as filler. First, sulfate anion-radicals generated by thermal dissociation of APS molecules not only abstract hydrogen atoms from hydroxyl groups of polysaccharide chains, but also can let the HSO_3 groups out from the polysaccharide structure because HSO_3 group is a good leaving group, resulting in the formation of alkoxy macroradicals. The good evidence for this claim is the disappearing of C-O-S related peak in FTIR spectrum that will be discussed in Sect. 3.2. In the next step, these macroradicals transfer own radical onto the nearest AA monomers, leading to the initiation and subsequent propagation of free-radical polymerization process. At this step, the vinyl groups of MBA molecules can react with graft polymer chains to form crosslinked polymeric network. During this process, linear PVP chains can penetrate into the hydrogel network by inter-molecular hydrogen-bonding interactions. Also, silica nanoparticles can create hydrogen bonds with functional groups of polymer chains, and thus can act as physical cross-linking agent.

3.2 FT-IR spectroscopy

FT-IR spectra of the prepared samples are shown in Fig. 1. In Fig. 1a which shows the characteristic peaks of CMC, a broad peak at 3400 cm^{-1} is related to the stretching vibration of $-\text{OH}$ group, peaks emerged at 2900 , 1060 , and 1620 cm^{-1} are attributed to the stretching vibration of methylene group, β -1,4-glycosidic bond, and carboxyl group, respectively [25]. Figure 1b shows characteristic absorption bands of SCMC. Absorption peaks appeared at 1263 and 813 cm^{-1} are related to the asymmetric stretching vibration of $\text{S}=\text{O}$ group, while its symmetric stretching vibration emerged at 1010 cm^{-1} as a sharp peak. Also, the strong peak at 1140 cm^{-1} is due to the symmetric stretching vibration of $\text{C}-\text{O}-\text{S}$ [26–28]. In Fig. 1c for silica nanoparticles, absorption bands appeared at 460 , 784 , and 1085 cm^{-1} are corresponded to angular deformation and symmetric and asymmetric stretching vibration of $\text{Si}-\text{O}-\text{Si}$ bonds, respectively. In Fig. 1d, decreased intensity of the peaks at 1000 – 1160 cm^{-1} region can be ascribed that the grafting process has occurred mostly on $\text{C}-\text{O}-\text{SO}_3\text{H}$

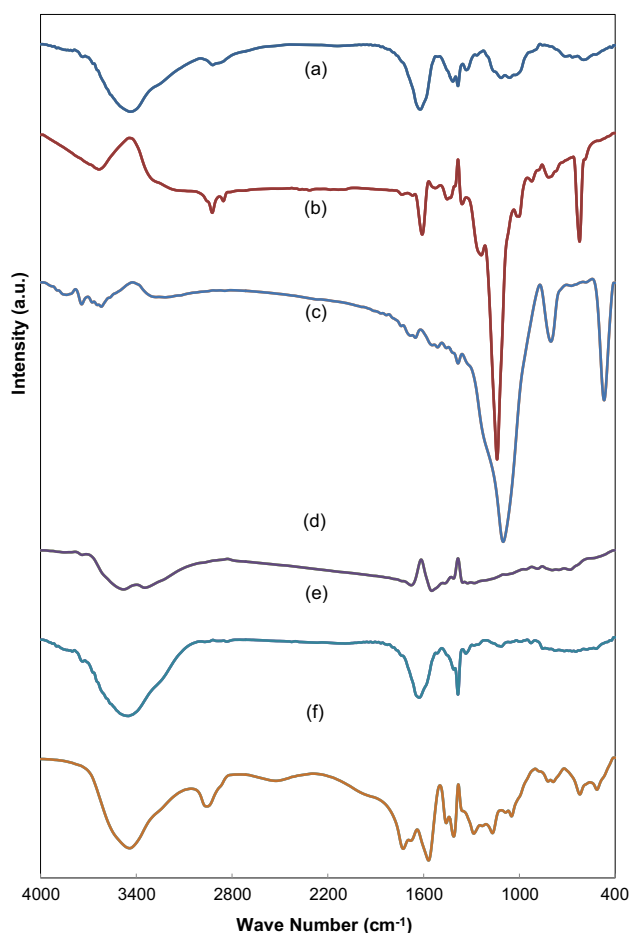


Fig. 1 FT-IR spectra of CMC (a), SCMC (b), silica (c), Hyd (d), Hyd/PVP (e) and Hyd/PVP/silica (f)

functional group while the HSO_3 is a better leaving group than H on OH functional group. So the characteristic peak of $\text{C}-\text{O}-\text{S}$ has severely weakened. Also, appearance of peak at 3400 cm^{-1} is related to stretching vibration of OH groups of AA which confirms the grafting reaction of AA onto SCMC chains. Since the PVP has $\text{C}-\text{N}$ bonds in its structure, the absorption band at 1282 cm^{-1} confirms the presence of PVP in hydrogel network (Fig. 2e) [29]. In Fig. 1f which is related to Hyd/PVP/silica superabsorbent nanocomposite, characteristic absorption peaks of silica are appeared, confirming that silica nanoparticles are incorporated into hydrogel network, successfully.

3.3 XRD patterns analysis

Figure 2 shows the XRD pattern of Hyd (a), Hyd/PVP (b), Hyd/PVP/silica superabsorbent nanocomposite (c), and silica (d). As shown in Fig. 2a, b, c broad peaks appeared at $2\theta = 22^\circ$ and 34° are related to amorphous structure of hydrogel. XRD pattern of silica (Fig. 2d) shows a broad

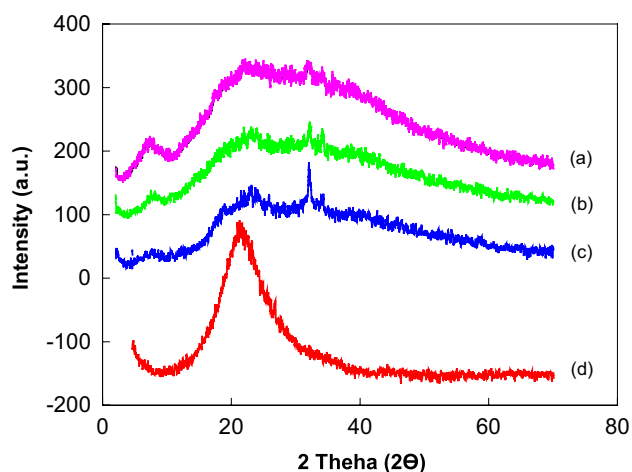


Fig. 2 XRD pattern of Hyd (a), Hyd/PVP (b) Hyd/PVP/silica (c) and silica (d)

peak at $2\theta = 21^\circ$, which is related to its amorphous structure [30]. This peak in Fig. 2c is eliminated which confirms that the silica nanoparticles are completely dispersed in the polymeric phase.

3.4 Surface morphology studies

Figure 3 shows SEM images of SCMC, Hyd, Hyd/PVP, and Hyd/PVP/silica superabsorbent nanocomposite. As depicted in Fig. 3a, b, SCMC has smooth surface. SEM image of Hyd (Fig. 3c, d) shows tighter and dense surface compared with the SCMC. Incorporation of PVP into polymeric matrix of Hyd causes to formation of porous structure, as seen in Fig. 3e and f. This can be attributed to the hydrophobic alkyl chain ends of PVP, which form tiny hydrophobic regions, generate ordered polymeric chains, and so build regular porous hydrogel network [22]. The porous structure of Hyd/PVP not only can enhance swelling rate, but also can improve its water uptake capacity. SEM images of Hyd/PVP/silica (Fig. 3g and h) show undulant porous structure. It can be clearly seen that incorporation of silica nanoparticles induces a reduction in porosity compared with the Hyd/PVP. Also, the EDX diffractogram of the Hyd/PVP/silica superabsorbent nanocomposite have been shown in Fig. 4. As evident in Fig. 4, superabsorbent nanocomposite contains carbon (C), oxygen (O), nitrogen (N), and silicon (Si) elements in own composition. The weight ratio of these elements has been shown as inset table in Fig. 4. These findings indicated that silica nanoparticle had been successfully incorporated

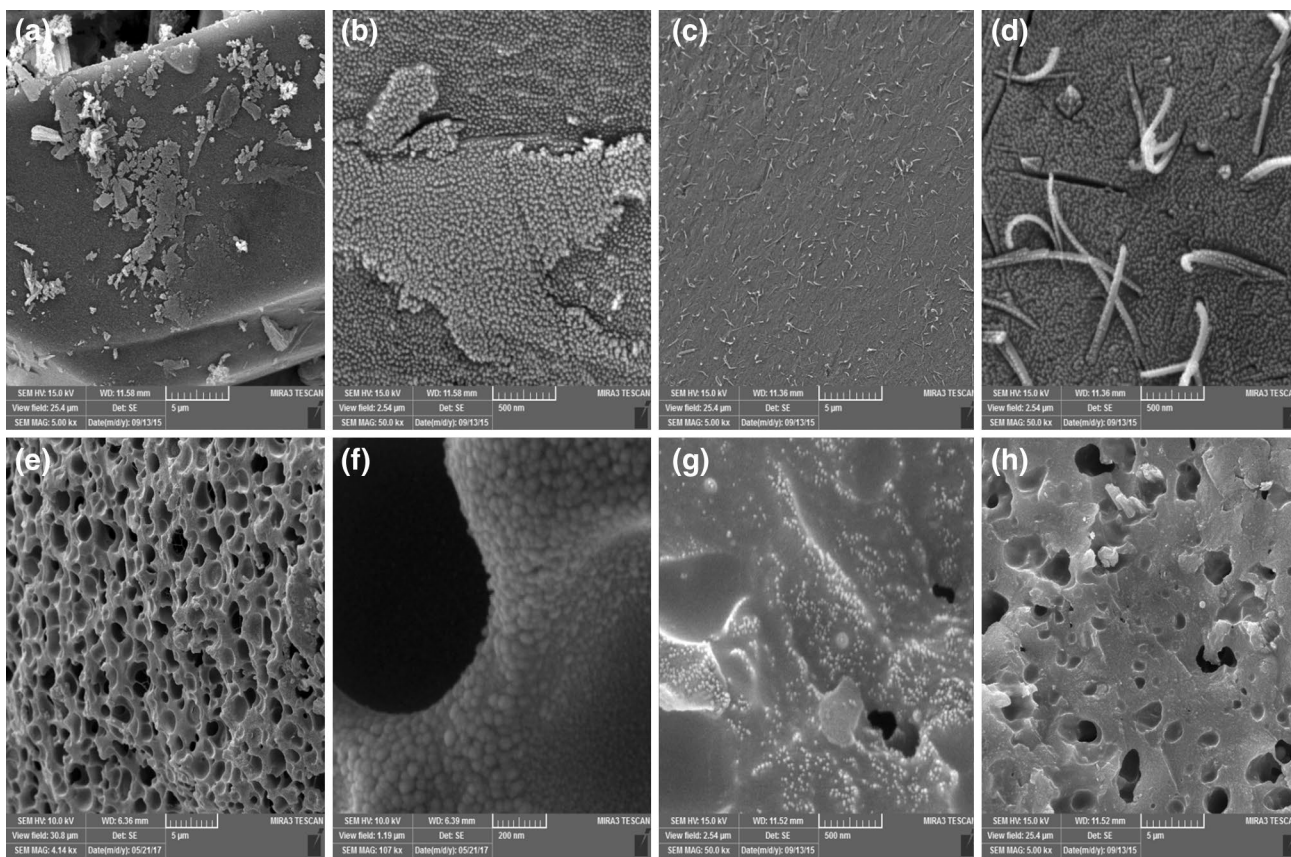


Fig. 3 SEM images of SCMC (a, b), Hyd (c, d), Hyd/PVP (e, f), and Hyd/PVP/silica (g, h)

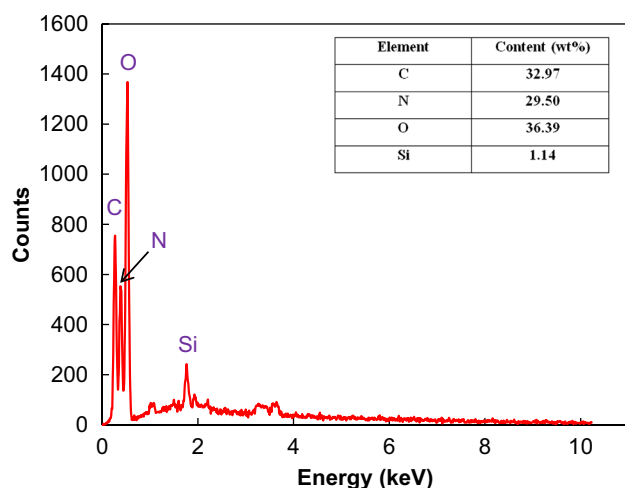


Fig. 4 EDX diffractogram of Hyd/PVP/silica sample (the inset table shows the weight ratio of the elements present in superabsorbent hydrogel composition)

into hydrogel matrix. Moreover, element mapping revealed that silica nanoparticles have homogeneous distribution throughout superabsorbent nanocomposite (Fig. 5).

3.5 TGA analysis

Thermogravimetric analysis (TGA) is an accurate and simple method for studying the thermal stability and decomposition pattern of polymers. Thus, the effect of PVP and silica nanoparticles presence on the thermal properties of superabsorbent nanocomposite was examined by TGA analysis under N_2 inert atmosphere. The thermal stability of

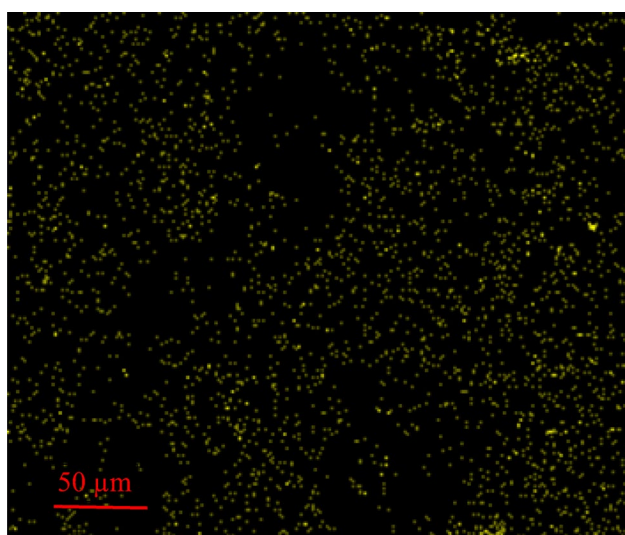


Fig. 5 Element mapping of silica nanoparticles on the surface of Hyd/PVP/silica sample

the neat hydrogel (Hyd) was compared with Hyd/PVP and Hyd/PVP/silica superabsorbent nanocomposite. The TGA curves of these hydrogels are shown in Fig. 6. The thermal decomposition mechanism of the hydrogels consists of three steps. The early minor weight loss is attributed to desorption of moisture as hydrogen bond of the water to the hydrogel structure. The second stage appears in the range of 360 and 400 °C. This weight loss could be assigned to decomposition of grafted poly(acrylic acid) chains. The main degradation temperature occurs between 450 and 500 °C. This step corresponds to decomposition of CMC and decarboxylation of previously formed anhydride groups [20, 31, 32]. As it is seen in TGA/DTG diagram of Hyd/PVP and Hyd/PVP/silica nanocomposites (Fig. 6), the second stage of weight loss which is related to the decomposition of grafted poly(acrylic acid) chains has been disappeared which confirms the effect of addition of PVP and silica on thermal stability of the hydrogel nanocomposite.

3.6 Effect of PVP content on equilibrium swelling capacity

To investigate the effect of PVP content on equilibrium swelling capacity of the hydrogels, different hydrogel samples with various PVP/SCMC weight ratios were synthesized. Figure 7a shows equilibrium swelling capacity of the hydrogel samples as a function of PVP/SCMC weight ratio. As shown in Fig. 7a, with increasing PVP/SCMC weight ratio from 0.5 to 1, equilibrium water absorption capacity increases. Further increment of PVP/SCMC weight ratio has reverse effect on equilibrium swelling capacity. The reason for enhancement of the swelling capacity at PVP/SCMC weight ratios lower than 1 can be interpreted as follow. PVP molecules can act as dispersant during polymerization reaction, resulting in the enhanced dispersion of reactants, and thus improved hydrogel network structure. Also, incorporation of non-ionic PVP chains into hydrogel network, due to its hydrophilic $-C=O(N)$ groups, increases

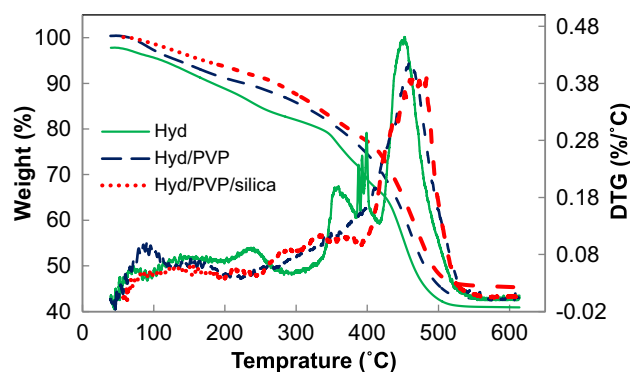


Fig. 6 TGA and DTG curves of Hyd, Hyd/PVP, and Hyd/PVP/silica

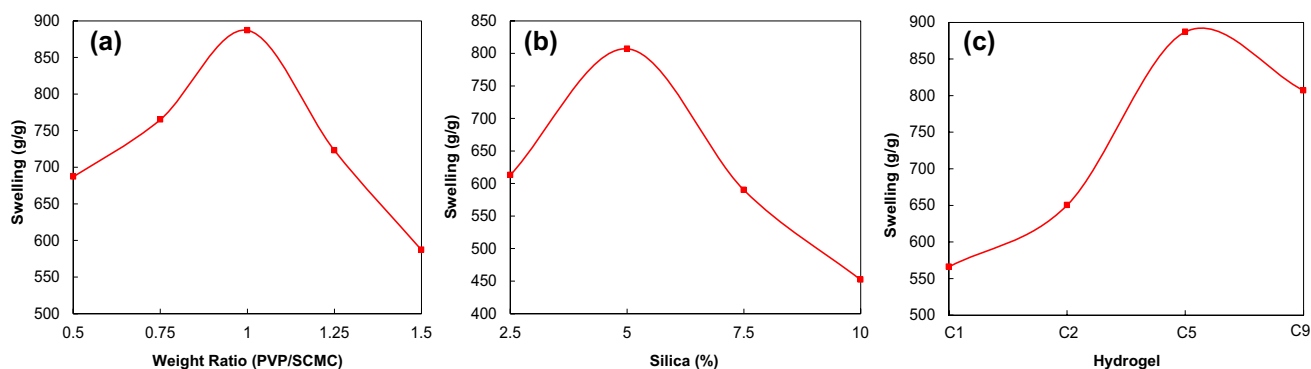


Fig. 7 Effect of PVP/SCMC weight ratio (a), silica content (b) on swelling capacity, and water absorption capacity of different hydrogel formulations (c)

the hydrophilicity of the synthesized hydrogel sample. Therefore, collaborative absorption effect of the hydrophilic groups in the hydrogel network leads to increased degree of swelling capacity. Moreover, hydrophobic alkyl chain ends of PVP form tiny hydrophobic regions, generate ordered polymeric chains, and thus make regular hydrogel network with improved swelling capacity [22]. At PVP/SCMC weight ratio higher than 1, PVP chains can tangle with the grafted polymer chains, leading to formation of physical crosslinking points within hydrogel network, and consequently reduced swelling capacity.

3.7 Effect of silica content on equilibrium swelling capacity

To study the effect of silica content on equilibrium swelling capacity of the hydrogels, different hydrogel samples with various silica amounts were synthesized. Figure 7b shows water absorption capacity of the hydrogel samples as a function of the silica content. As seen in this figure, the equilibrium water absorption capacity increases with increasing silica content up to 5 wt%. However, at silica contents higher than 5 wt%, the equilibrium water absorption capacity decreases. This can be attributed to the physical crosslinking effect of the silica nanoparticles. On the other hand, higher silica content results in higher crosslinking densities and subsequent decrement in water absorption capacity.

Figure 7c shows equilibrium water absorption capacity of CMC-g-poly(AA) (C₁), Hyd (C₂), Hyd/PVP (C₅), and Hyd/PVP/Silica (C₉) hydrogel samples. As it is obvious, C₂ has higher swelling capacity compared with the C₁. This can be attributed to the greater hydrophilicity of SCMC compared with the CMC, which ensures the higher swelling degree for SCMC-based hydrogels. Incorporation of PVP into SCMC-based hydrogel matrix (sample C₅), due to the introduction of more hydrophilic groups, generates a hydrogel network with higher swelling capacity. Nevertheless, the swelling

capacity decreases by introducing silica nanoparticles within hydrogel network (sample C₉). In fact, physical crosslinking effect of the incorporated silica nanoparticles increases the crosslinking density, leading to the shrank hydrogel network, and reduced swelling capacity.

3.8 Effect of solution pH on swelling behavior

Swelling behavior of the Hyd/PVP/silica superabsorbent nanocomposite was evaluated in different pH solutions ranging from 2 to 12. As shown in Fig. 8, the equilibrium swelling capacity increases with increasing pH values from 2 to 4, and then it remained almost constant in the pH range of 4–10. Further increase in pH values up to 12 resulted in a reduction of swelling capacity. The observed trend in swelling behavior at different pH solutions can be explained as follow. At pH values lower than 4, all carboxyl and sulfonate groups are protonated, leading to the strength

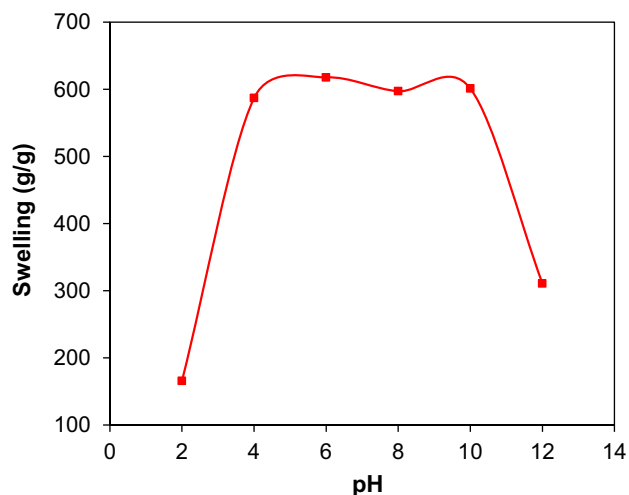


Fig. 8 Effect of pH on swelling capacity of hydrogel

hydrogen-bonding interactions, generation of additional physical cross-linkages in the hydrogel network, and consequently reduced swelling capacity. By increasing pH values from 4 to 10, due to the de-protonation of carboxylic and sulfonic acid groups, hydrogen-bonding interactions are broken. Besides, dissociation of the carboxylic and sulfonic acid groups can reinforce anion–anion repulsions among carboxylate and sulfonate groups, which result in an expanded hydrogel network and higher swelling capacity. Reduction of the equilibrium swelling capacity at pH values higher than 10 is related to the shielding effect of Na^+ counter-ions on the carboxylate and sulfonate anions, which effectively hinders anion–anion repulsions among them. Therefore, hydrogel network tends to shrink, and thus swelling capacity decreases [33, 34].

3.9 Effect of salt solution on swelling behavior

To investigate the effect of concentration of saline solutions on the swelling ratio of Hyd/PVP/silica superabsorbent nanocomposite, its swelling behavior was assessed in various aqueous solutions of NaCl with different concentrations (Fig. 9a). Also, the effect of type of saline solutions on the swelling behavior of the superabsorbent nanocomposite was evaluated by measuring its swelling capacity in 1 M aqueous solutions of NaCl, CaCl_2 , and FeCl_3 (Fig. 9b). As shown in Fig. 9a, swelling capacity of the superabsorbent nanocomposite sample decreased as the concentration of the saline solutions increased. This can be explained by osmotic pressure phenomenon. High concentration of the external saline solutions decreases osmotic pressure difference between hydrogel matrix and swelling medium, resulting in a reduced swelling capacity. Moreover, with rising salt concentration, shielding effect of the cations on carboxylate and sulfonate anions

increases, which severely restricts effective anion–anion repulsions among carboxylate and sulfonate groups. Consequently, hydrogel network shrinks and swelling capacity decreases. As shown in Fig. 9b, the equilibrium swelling capacity of the hydrogel nanocomposite sample in different saline solutions was in the order of $\text{Na}^+ > \text{Ca}^{2+} > \text{Fe}^{3+}$. This phenomenon can be justified as follow. In the presence of multivalent cations (Ca^{2+} and Fe^{3+}), due to the complexation of carboxylate and sulfonate anions by these cations, ionic crosslinking density of the hydrogel network increases, leading to the decreased swelling capacity [35]. Moreover, greater electrostatic attractions of Fe^{3+} cations with anionic groups compared with those in Ca^{2+} cations induce higher degree of ionic crosslinking density within hydrogel network. Therefore, water uptake capacity of the hydrogel nanocomposite sample in FeCl_3 aqueous solution was less than that of value in CaCl_2 aqueous solution [36].

3.10 Swelling kinetic studies

The effect of sulfonation, PVP and silica addition on the water absorption capacity and swelling kinetic of the CMC based hydrogels was studied. As shown in Fig. 10, all hydrogel samples exhibit similar trend, in which the swelling ratio substantially increases at initial time periods and then the rate of swelling decreases to reach equilibrium swelling capacity. According to the swelling kinetic curves, the equilibrium swelling capacity of C_1 , C_2 , C_5 , and C_9 was about 566, 650.2, 887, and 807 g/g, respectively.

To investigate the swelling kinetic of the hydrogel samples, the second order kinetic equation proposed by Schott, is used [37].

$$\frac{t}{W} = A + Bt \quad (2)$$

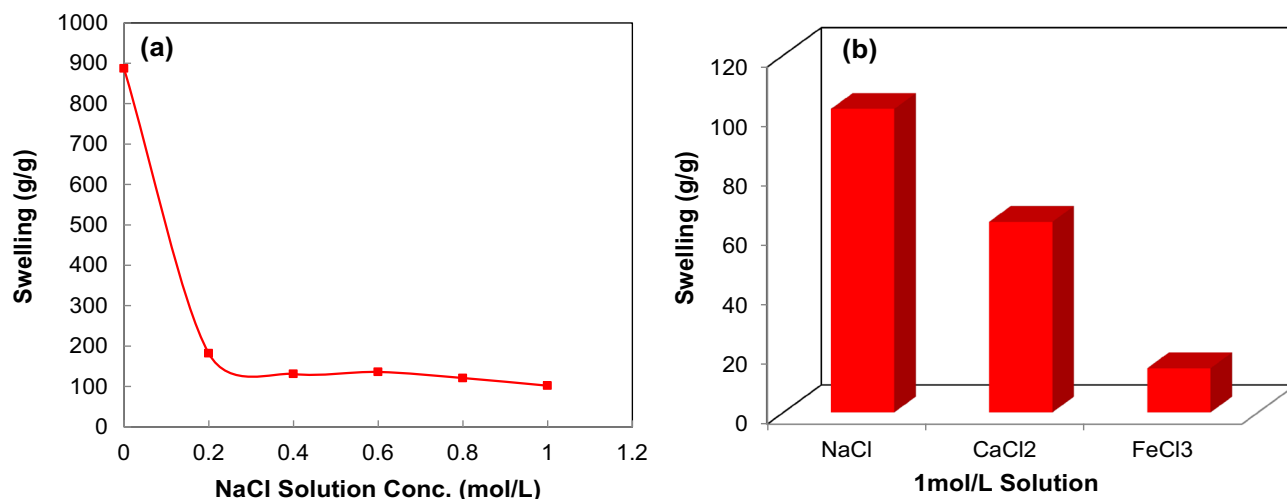


Fig. 9 Effect of NaCl solution concentration (a) and saline solution type (b) on swelling capacity of hydrogel

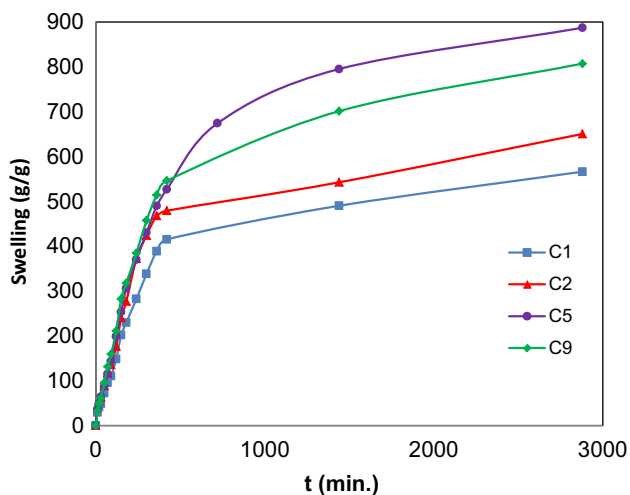


Fig. 10 Swelling kinetic of prepared hydrogels

$$B = \frac{1}{W_\infty} \tag{3}$$

$$A = \frac{1}{\left(\frac{dW}{dt}\right)_0} \tag{4}$$

$$k_s = \frac{1}{AW_\infty^2} \tag{5}$$

where, W and W_∞ are water absorption capacity at time t (min) and at equilibrium, respectively. B is the reverse of the theoretical equilibrium swelling capacity, A (g min/g) is the reverse of the initial swelling rate, and k_s (g/g min) is the swelling rate constant. Plotting t/W versus t gives straight line which is demonstrated in Fig. 11a. The slope and intercept of the plotted straight lines were used to determine W_∞ and k_s , respectively. The values of these parameters are presented in Table 2. The theoretical water absorption capacities (W_∞) achieved for C_1 (588.23 g/g), C_2 (769.23 g/g), C_5 (1000 g/g), and C_9 (999.09 g/g) were found to be very close to those values obtained experimentally. In addition, the highest swelling rate constant was achieved for C_5 . This can be attributed to the porous structure of C_5 , which provides more contact surface area for water molecules, facilitate water diffusion process, and so increases swelling rate.

To study the water diffusion nature of the hydrogel samples, the following equation was used which is reliable for the first 60% of the fractional water uptake [38].

$$\frac{W_t}{W_\infty} = kt^n \tag{6}$$

where W_t and W_∞ are the swelling capacity at time t (min) and at equilibrium state, respectively. Parameter k is the specific proportionality constant of hydrogel and n determines the water diffusion mechanism. For fickian diffusion mechanism, n is in the range of 0.45–0.5, and for non-fickian diffusion mechanism it is a value between 0.5 and 1. In case-II diffusion, or relaxation-controlled release, n is equal to 1, and in supercase-II diffusion, n is greater than 1 [39]. Figure 11b shows the plot of $\ln(W_t/W_\infty)$ versus $\ln(t)$. Parameters n and k were determined from the slope and intercept of the plotted curve, respectively, and are reported in Table 2. According to this table, the values of n for hydrogel (C_2) and hydrogel nanocomposite sample (C_9) was 0.79 and 0.98, respectively, indicating that water diffusion mechanism for both hydrogels follows non-Fickian diffusion type.

Diffusion coefficient of the hydrogel samples is another parameter which is used to characterize their swelling behavior. To determine this parameter, short time approximation method was used. This method is reliable for initial 60% of swelling ratio. Diffusion coefficient for spherical hydrogel samples is obtained using the following Equation [40]:

$$\frac{W_t}{W_\infty} = 4\left(\frac{D \times t}{\pi r^2}\right)^{(1/2)} \tag{7}$$

In this equation, D (cm²/min) is diffusion coefficient, t (min) is time, and r (cm) is the radius of the spherical hydrogel samples. By comparing Eq. 6 with Eq. 7 and considering $n = 0.5$, the following equation can be obtained:

$$k = 4\left(\frac{D}{\pi r^2}\right)^{1/2} \tag{8}$$

Plotting W_t/W_∞ versus $t^{1/2}$ gives straight line (Fig. 11c), which diffusion coefficient (D) value was determined from its slope. According to the obtained results (Table 2), diffusion coefficient of the hydrogel nanocomposite sample (C_9) (3.53×10^{-10} cm² min⁻¹) was greater than that of neat hydrogel sample (2.07×10^{-7} cm² min⁻¹). This implies that water molecules diffuse into hydrogel nanocomposite network faster than that of hydrogel sample. The highly porous structure of the hydrogel nanocomposite sample made by incorporated PVP is responsible for this phenomenon.

Another important parameter to evaluate the diffusional characteristics of the hydrogel samples is water absorption rate which is calculated using the following Equation [41]:

$$W_t = W_\infty(1 - e^{-k_w t}) \tag{9}$$

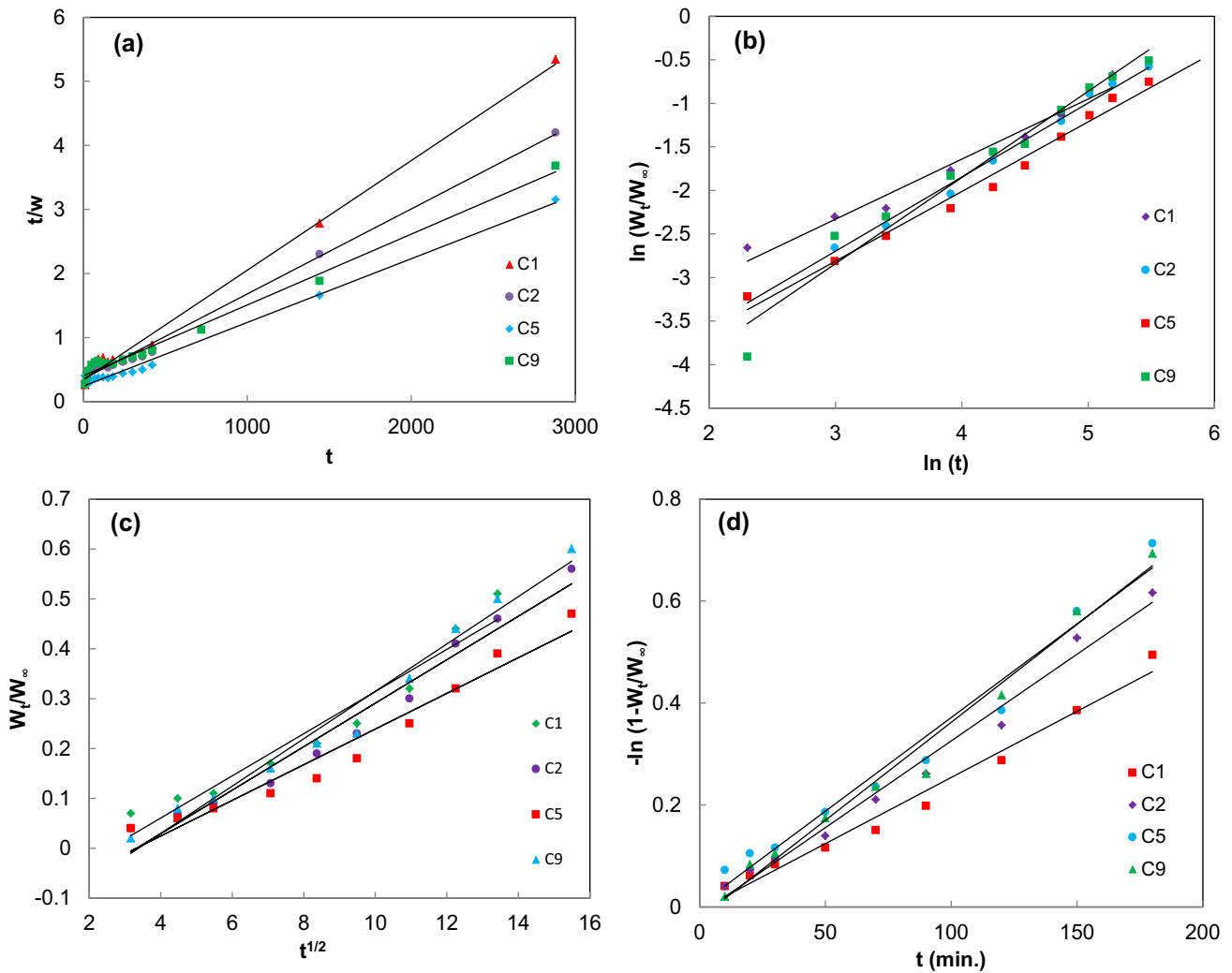


Fig. 11 Swelling kinetic curves of prepared hydrogels

Table 2 Swelling kinetic and diffusion parameters of prepared hydrogels

| Sample | Swelling kinetic parameters | | | | | |
|----------------|-----------------------------|------------|--------|------|------------------------|--------|
| | K_s | W_∞ | k | n | D | k_w |
| C ₁ | 8.52×10^{-6} | 588.23 | 0.0129 | 0.69 | 1.74×10^{-10} | 0.0026 |
| C ₂ | 3.79×10^{-5} | 769.23 | 0.0022 | 0.79 | 2.07×10^{-10} | 0.0034 |
| C ₅ | 9.36×10^{-5} | 1000 | 0.0052 | 0.80 | 2.40×10^{-10} | 0.0037 |
| C ₉ | 8.99×10^{-5} | 999.09 | 0.0059 | 0.98 | 3.53×10^{-10} | 0.0038 |

where W_t and W_∞ are the water absorption capacity at time t (min) and at equilibrium, respectively. Parameter t is the water absorption time (min) and k_w is the water absorption rate constant. By using the above equation and plotting $-\ln(1 - W_t/W_\infty)$ versus t Fig. 11d, k_w was determined from the slope of the plotted straight line, which the results are reported in Table 2. It can be seen that water absorption rate constant for hydrogel sample (0.0034) is less than that

of hydrogel nanocomposite sample (0.0038). These results showed that water absorption rate in hydrogel nanocomposite sample is higher than that of hydrogel sample, which is in good agreement with previously obtained results.

4 Conclusions

A novel hydrogel nanocomposite was synthesized by free-radical graft polymerization of acrylic acid onto sulfonated CMC in the presence of PVP and silica nanoparticles. FTIR analysis results confirmed that graft polymerization of acrylic acid onto SCMC as well as incorporation of PVP into hydrogel network was performed successfully. Also, SEM images showed that incorporation of PVP into hydrogel matrix leads to formation of porous structure. Porous structure of the hydrogel nanocomposite sample caused greater water absorption capacity and higher swelling rate compared with the neat hydrogel sample. Moreover, hydrogel nanocomposite presented good pH-responsive and salt sensitivity behavior. Such good characteristics revealed that Hyd/PVP/Silica superabsorbent nanocomposite can be suitable for agricultural and horticultural applications.

Acknowledgements The financial support of this work by the University of Tabriz is gratefully acknowledged.

Funding This study was funded by Department of Applied Chemistry, Faculty of Chemistry, University of Tabriz, Tabriz, Iran.

Compliance with ethical standards

Conflict of interest The authors declare that they have no conflict of interest.

References

- M. Rasoulzadeh, H. Namazi, *Carbohydr. Polym.* **168**, 320 (2017)
- Y. Zhou, S. Fu, L. Zhang, H. Zhan, *Carbohydr. Polym.* **97**(2), 429 (2013)
- K. Hemvichian, A. Chanthawong, P. Suwanmala, *Radiat. Phys. Chem.* **103**, 167 (2014)
- A. Rashidzadeh, A. Olad, D. Salari, A. Reyhanitabar, *J. Polym. Res.* **21**(2), 1 (2014)
- S. Spoljaric, A. Salminen, N.D. Luong, J. Seppälä, *Eur. Polym. J.* **56**, 105 (2014)
- W. Zhang, X. Wang, J. Ma, L. Zhao, C. Yang, K. Wang, X. Pu, Y. Wang, F. Ran, Y. Wang, *J. Porous Mater.* **24**(2), 497 (2017)
- M. Yu, J. Li, L. Wang, *J. Porous Mater.* **23**(4), 997 (2016)
- G. Marci, G. Mele, L. Palmisano, P. Pulito, A. Sannino, *Green Chem.* **8**(5), 439 (2006)
- S. Pan, A.J. Ragauskas, *Carbohydr. Polym.* **87**(2), 1410 (2012)
- T. Patra, A. Pal, J. Dey, *Langmuir* **26**(11), 7761 (2010)
- A. Pourjavadi, M. Doulabi, A.A. Alamolhoda, E. Tavakkoli, S. Amirshakari, *J. Appl. Polym. Sci.* **130**(4), 3001 (2013)
- T. Fekete, J. Borsa, E. Takács, L. Wojnárovits, *Carbohydr. Polym.* **166**, 300 (2017)
- T. Fekete, J. Borsa, E. Takács, L. Wojnárovits, *Radiat. Phys. Chem.* **124**, 135 (2016)
- H.A. Essawy, M.B. Ghazy, F.A. El-Hai, M.F. Mohamed, *Int. J. Biol. Macromol.* **89**, 144 (2016)
- A. Pourjavadi, R. Soleyman, H. Ghasemzadeh, H. Salimi, *Iran. Polym. J.* **19**(8), 571 (2010)
- A. Bortolin, F.A. Aouada, L.H. Mattoso, C. Ribeiro, *J. Agric. Food. Chem.* **61**(31), 7431 (2013)
- H. Gad, N.A. Maziad, *Int. J. Adv. Sci. Tech. Res.* **4**(4), 184 (2014)
- A. Rashidzadeh, A. Olad, *Carbohydr. Polym.* **114**, 269 (2014)
- S. Chandrasekhar, P. Pramada, L. Praveen, *J. Mater. Sci.* **40**(24), 6535 (2005)
- H. Gharekhani, A. Olad, A. Mirmohseni, A. Bybordi, *Carbohydr. Polym.* **168**, 1 (2017)
- A. Pourjavadi, F. Seidi, H. Salimi, R. Soleyman, *J. Appl. Polym. Sci.* **108**(5), 3281 (2008)
- W. Wang, A. Wang, *Carbohydr. Polym.* **80**, 4, 1028 (2010)
- N. Roy, N. Saha, T. Kitano, P. Saha, *J. Appl. Polym. Sci.* **117**(3), 1703 (2010)
- A. Olad, H. Gharekhani, A. Mirmohseni, A. Bybordi, *Polym. Bull.* **74**(8), 3353 (2017)
- F. Wu, Y. Zhang, L. Liu, J. Yao, *Carbohydr. Polym.* **87**(4), 2519 (2012)
- J. Yang, Y. Du, R. Huang, Y. Wan, T. Li, *Int. J. Biol. Macromol.* **31**(1), 55 (2002)
- B. Matsuhira, P. Rivas, *J. Appl. Phycol.* **5**(1), 45 (1993)
- C. Mähner, M.D. Lechner, E. Nordmeier, *Carbohydr. Res.* **331**(2), 203 (2001)
- N. Arsalani, H. Fattahi, M. Nazarpour, *eXPRESS Polym. Lett.* **4**(6), 329 (2010)
- N. Yalcin, V. Sevinc, *Ceram. Int.* **27**(2), 219 (2001)
- M. Zohuriaan, F. Shokrolahi, *Polym. Test.* **23**(5), 575 (2004)
- S. El-Sayed, K. Mahmoud, A. Fatah, A. Hassen, *Phys. B* **406**, 21, 4068 (2011)
- J.D.S. Cândido, A.G. Pereira, A.R. Fajardo, N.M. Ricardo, J.P. Feitosa, E.C. Muniz, F.H. Rodrigues, *Compos. Part B* **51**, 246 (2013)
- C. Spagnol, F.H. Rodrigues, A.G. Pereira, A.R. Fajardo, A.F. Rubira, E.C. Muniz, *Carbohydr. Polym.* **87**(3), 2038 (2012)
- A. Pourjavadi, H. Ghasemzadeh, R. Soleyman, *J. Appl. Polym. Sci.* **105**(5), 2631 (2007)
- G.B. Marandi, G.R. Mahdavinia, S. Ghafary, *J. Polym. Res.* **18**(6), 1487 (2011)
- H. Schott, *J. Macromol. Sci. Part B* **31**(1), 1 (1992)
- S. Li, X. Liu, T. Zou, W. Xiao, *CLEAN–Soil, Air, Water* **38**(4), 378 (2010)
- H. Kaşgöz, A. Durmus, *Polym. Adv. Technol.* **19**(7), 838 (2008)
- E. Karadağ, ÖB. Üzümlü, D. Saraydin, *Mater. Des.* **26**(4), 265 (2005)
- T. Singh, R. Singhal, *J. Appl. Polym. Sci.* **125**(2), 1267 (2012)